

Supplementary Information

Implementation of 2,2'-azobispyridine radical mono- and dianions in dinuclear rare earth metal complexes

Francis Delano IV and Selvan Demir*

Department of Chemistry, Michigan State University, 578 South Shaw Lane, East Lansing, Michigan 48824, USA

*Correspondence to: sdemir@chemistry.msu.edu (S.D.)

Table of Contents

| | |
|--|------------|
| Materials and Methods | S4 |
| X-ray Crystallography | S8 |
| Table S1. Crystal data and structure refinement of $[(\text{Cp}^{\text{tet}}_2\text{Y})_2(\mu\text{-abpy})]$, 1 , and $[(\text{Cp}^{\text{tet}}_2\text{Y})_2(\mu\text{-abpy}^*)](\text{BPh}_4)$, 2 | S8 |
| Figure S1. Structure of $[(\text{Cp}^{\text{tet}}_2\text{Y})_2(\mu\text{-abpy})]$, 1 | S9 |
| Figure S2. Structure of $[(\text{Cp}^{\text{tet}}_2\text{Y})_2(\mu\text{-abpy})]$, 1 , with thermal ellipsoids | S9 |
| Figure S3. Structure of $[(\text{Cp}^{\text{tet}}_2\text{Y})_2(\mu\text{-abpy})]$, 1 , with atom labels | S10 |
| Figure S4. Structure of the cation of $[(\text{Cp}^{\text{tet}}_2\text{Y})_2(\mu\text{-abpy}^*)](\text{BPh}_4)$, 2 | S10 |
| NMR Spectroscopy | S11 |
| Figure S5. ^1H NMR spectrum of $[(\text{Cp}^{\text{tet}}_2\text{Y})_2(\mu\text{-abpy})]$, 1 | S11 |
| Figure S6. ^{13}C NMR spectrum of $[(\text{Cp}^{\text{tet}}_2\text{Y})_2(\mu\text{-abpy})]$, 1 | S11 |
| Figure S7. ^1H - ^1H gCOSY spectrum of $[(\text{Cp}^{\text{tet}}_2\text{Y})_2(\mu\text{-abpy})]$, 1 | S12 |
| Figure S8. ^1H - ^{13}C gHSQC spectrum of $[(\text{Cp}^{\text{tet}}_2\text{Y})_2(\mu\text{-abpy})]$, 1 | S12 |
| Figure S9. ^1H NMR spectrum of the crude reaction mixture for the synthesis of $[(\text{Cp}^{\text{tet}}_2\text{Y})_2(\mu\text{-abpy})]$, 1 | S13 |
| Figure S10. ^1H NMR spectrum of $[(\text{Cp}^{\text{tet}}_2\text{Y})_2(\mu\text{-abpy}^*)](\text{BPh}_4)$, 2 | S13 |
| IR Spectroscopy | S14 |
| Figure S11. FTIR spectrum of $[(\text{Cp}^{\text{tet}}_2\text{Y})_2(\mu\text{-abpy})]$, 1 | S14 |
| Figure S12. FTIR spectrum of $[(\text{Cp}^{\text{tet}}_2\text{Y})_2(\mu\text{-abpy}^*)](\text{BPh}_4)$, 2 | S14 |
| UV-vis Spectroscopy | S15 |
| Figure S13. UV-vis spectra of $[(\text{Cp}^{\text{tet}}_2\text{Y})_2(\mu\text{-abpy})]$, 1 , and $[(\text{Cp}^{\text{tet}}_2\text{Y})_2(\mu\text{-abpy}^*)](\text{BPh}_4)$, 2 | S15 |
| Figure S14. UV-vis spectra of $[(\text{Cp}^{\text{tet}}_2\text{Y})_2(\mu\text{-abpy})]$, 1 , with calculated transitions | S15 |
| Figure S15. UV-vis spectra of $[(\text{Cp}^{\text{tet}}_2\text{Y})_2(\mu\text{-abpy}^*)](\text{BPh}_4)$, 2 with calculated transitions | S16 |
| Cyclic Voltammetry | S17 |
| Figure S16. Cyclic voltammogram of $[(\text{Cp}^{\text{tet}}_2\text{Y})_2(\mu\text{-abpy})]$, 1 , in dichloromethane | S17 |
| DFT Calculations | S18 |
| Table S2. Computed and average experimental bond metrics of 2 | S18 |

| | |
|---|------------|
| Figure S17. Comparison of experimental FTIR spectrum and calculated stretching frequencies of 1 | S19 |
| Figure S18. Calculated frontier orbitals of $[(\text{Cp}^{\text{tet}_2\text{Y}})_2(\mu\text{-abpy})]$, 1 | S19 |
| Figure S19. Comparison of experimental FTIR spectrum and calculated stretching frequencies of 2 | S20 |
| Figure S20. Calculated frontier orbitals of $[(\text{Cp}^{\text{tet}_2\text{Y}})_2(\mu\text{-abpy}^*)](\text{BPh}_4)$, 2 | S20 |
| Figure S21. Calculated Mulliken spin densities of $[(\text{Cp}^{\text{tet}_2\text{Y}})_2(\mu\text{-abpy}^*)](\text{BPh}_4)$, 2 | S21 |
| Table S3. Major contributions of TDDFT calculated transitions for 1 | S22 |
| Table S4. Major contributions of TDDFT calculated transitions for 2 | S24 |
| Table S5. Comparison of calculated and experimental hyperfine coupling constants of 2 | S25 |
| References | S26 |

Materials and Methods

General Information

All manipulations described below were performed under an inert N₂ or Ar atmosphere with rigorous exclusion of oxygen and moisture using Schlenk and glovebox techniques. House nitrogen was purified through a MBraun HP-500-MO-OX gas purifier prior to use. Toluene was dried by refluxing over potassium using benzophenone as an indicator and distilled prior to use. *n*-Hexane, dichloromethane, and diethyl ether were dried by refluxing over calcium hydride and distilled prior to use. Allylmagnesium chloride, 6% sodium hypochlorite solution, and anhydrous YCl₃ were purchased from Sigma-Aldrich and used without further purification. Tetramethylcyclopentadiene (Cp^{tet}H) was purchased from Sigma-Aldrich and dried over 4 Å sieves prior to use. 2-aminopyridine was purchased from Alfa-Aesar and used as received. Potassium bis(trimethylsilyl)amide, KN[Si(CH₃)₃]₂, was purchased from Sigma-Aldrich, dissolved in toluene, filtered through a Celite plug, and recrystallised from toluene at -35 °C. The compounds KCp^{tet},¹ [HNEt₃][BPh₄],² KC₈,³ 2,2-azobispyridine (abpy),⁴ [Cp₂Fe][BPh₄],⁵ and Cp^{tet}₂Y(BPh₄),⁶ were prepared according to literature procedures. A PerkinElmer 2400 Series II CHNS/O analyzer was used for CHN elemental analyses. IR spectra were obtained through use of a Cary 630 diamond ATR-IR spectrometer in a dinitrogen atmosphere. UV-vis data were collected on an Agilent Cary60, in a 1 cm cuvette equipped with a Schlenk adaptor.

Synthesis of [(Cp^{tet}₂Y)₂(μ-abpy)], 1. In a 20 mL scintillation vial, 133 mg (0.20 mmol) of Cp^{tet}₂Y(BPh₄) was suspended in 12 mL of toluene and subsequently heated to 90 °C for 15 minutes. Once Cp^{tet}₂Y(BPh₄) was completely dissolved, a bright red 0.5 mL toluene solution containing 19 mg (0.10 mmol) of abpy was added dropwise to the stirring metal solution at 90 °C, accompanied by the immediate formation of a deep purple solution. After two minutes, 28 mg (0.21 mmol) of KC₈ was added, and the reaction was allowed to proceed at 90 °C. As the reaction progresses a gradual color change from deep purple to bright red is observed. After 16 hours, heating was stopped, and the reaction mixture was allowed to cool to room temperature. The resulting reaction mixture was centrifuged, and the bright red supernatant was filtered through a Kimwipe plug. Notably, filtration of the supernatant through Celite results in discoloration of the Celite, indicative of decomposition. All toluene was removed under reduced pressure, resulting in a bright-red oily residue. The ¹H NMR spectrum of the crude reaction mixture points to additional reduction processes originating from the ancillary [BPh₄]⁻ motif, as evidenced by the presence of resonances attributed to both biphenyl and BPh₃, Figure S9. Similar reduction processes have been observed for Cp*₂Y(BPh₄) (Cp* = pentamethylcyclopentadienyl).⁷ The residue was washed with two 0.5 mL portions of hexane, and the resulting orange solid was dried under vacuum for 30 minutes. The solid was dissolved in toluene at 90 °C, filtered through a Kimwipe plug, and stored at -35 °C for crystallisation. Red crystals suitable for single-crystal X-ray diffraction analysis were grown over the course of three days in 20% crystalline yield (17.4 mg, 0.02 mmol). ¹H NMR (500 MHz, ppm, benzene-*d*₆, 25 °C): δ 1.91 (s, 12 H, C₅Me₄H), 1.92 (s, 12 H, C₅Me₄H), 2.03 (s, 12 H, C₅Me₄H), 2.09 (s, 12 H, C₅Me₄H), 5.10 (d, ³J_{H-H} = 8.85 Hz, 2 H,

abpy-H_A), 5.78 (t, ³J_{H-H} = 6.24 Hz, 2 H, abpy-H_C), 5.97 (s, 4 H, C₅Me₄H), 6.69 (td, ³J_{H-H} = 7.54 Hz, ⁴J_{H-H} = 1.61 Hz, 2 H, abpy-H_B), 6.90 (d, ³J_{H-H} = 5.78 Hz, 2 H, abpy-H_D). ¹³C NMR (126 MHz, ppm, benzene-*d*₆, 25 °C): δ 11.60 (C₅Me₄H), 11.68 (C₅Me₄H), 13.42 (C₅Me₄H), 13.65 (C₅Me₄H), 105.66 (abpy-C_C), 111.77 (abpy-C_E), 112.32 (abpy-C_A), 117.16 (C₅Me₄H), 118.20 (C₅Me₄H), 120.59 (C₅Me₄H), 121.17 (C₅Me₄H), 134.46 (abpy-C_B), 143.56 (abpy-C_D), 158.75 (C₅Me₄H). See Figure S3 for relevant atom labels. Anal. Calcd for C₄₆H₆₀N₄Y₂: C, 65.24; H, 7.14; N, 6.62. Found: C, 65.45; H, 6.84; N 6.69. IR (ATR, cm⁻¹): 3050w, 2899m, 2859m, 1613s, 1477s, 1438s, 1373s, 1270m, 1160m, 1108w, 1023w, 986s, 884w, 854w, 781m, 748m, 698m.

Synthesis of [(Cp^{tet}Y)₂(μ-abpy)](BPh₄), 2. In a 20 mL scintillation vial, 17 mg (0.02 mmol) of **1** was dissolved in 6 mL of Et₂O and cooled to -78 °C. A 2 mL suspension containing 10 mg (0.02 mmol) of [Cp₂Fe][BPh₄] was added dropwise to the bright red reaction mixture at -78 °C, accompanied by the immediate appearance of a deep purple solution. The reaction was allowed to proceed at -78 °C. After 90 minutes, the volatiles were removed under reduced pressure and the resulting purple residue was washed with four 1 mL portions of toluene, and subsequently dried under vacuum revealing an oily solid. Crystals suitable for single-crystal X-ray diffraction analysis were grown from slow evaporation of a 1:1 dichloromethane:toluene solution at -35 °C in 41% yield (10 mg, 0.01 mmol). ¹H NMR (500 MHz, ppm, THF-*d*₈, 25 °C) δ: 7.34, 7.20, 7.18, 7.17, 7.13, 7.12, 7.07, 6.87, 6.72, 2.30, 2.15, 1.97, 1.73. The paramagnetic nature of [(Cp^{tet}Y)₂(μ-abpy)](BPh₄) results in significant peak broadening in the ¹H-NMR spectrum, Figure S10, thus, signals were not integrated or assigned. Drying of the resulting crystalline material results in removal of all co-crystallised solvent molecules. Compound **2** is ¹³C NMR silent. Anal. Calcd for C₇₀H₈₀BN₄Y₂: C, 72.10; H, 6.92; N, 4.80. Found: C, 72.30; H, 6.87; N, 4.48. IR (ATR, cm⁻¹): 3053w, 2904m, 2858m, 1592w, 1544s, 1462s, 1428m, 1382w, 1308m, 1244w, 1162m, 1111w, 1067w, 1030w, 1003s, 846w, 773m, 711m.

X-ray Crystallography

Data were collected on a XtaLAB Synergy, Dualflex, HyPix diffractometer using Cu Kα radiation. Red and black block-shaped crystals with dimensions 0.187 × 0.138 × 0.105 mm³, and 0.221 × 0.143 × 0.063 mm³ for **1** and **2**, respectively, were suspended in *n*-Paratone oil and mounted on a nylon loop. The temperature was controlled through use of an Oxford Cryosystems low-temperature device, operating at 100 K.

The data collection strategy, unit cell determination, and data reduction were performed by the CrysAlisPro software,⁸ which corrects for Lorentz-polarization. Absorption effects were accounted for through use of a numerical absorption correction based on Gaussian integration over a multifaceted crystal model using spherical harmonics implemented in the SCALE3 ABSPACK⁹ scaling algorithm.

The structure of **1** and **2** were solved in the space group *P*2₁/*n* by using dual methods with ShelXT¹⁰ and refined by least squares using version 20189/2 of XL¹¹ incorporated in Olex2.¹² All non-hydrogen atoms were refined anisotropically. Hydrogen atom positions were calculated geometrically and refined using the riding model. The structure of **2** exhibits considerable molecular disorder concerning the central abpy unit. To simplify the structural discussion, only the majority contribution was discussed in the manuscript.

NMR Spectroscopy

All NMR spectra were recorded on a Bruker Avance III HD 500 MHz NMR spectrometer in benzene- d_6 or THF- d_8 . NMR samples were prepared under an argon atmosphere and sealed using J-Young tubes. Benzene- d_6 was purchased from Sigma-Aldrich and dried over 4 Å molecular sieves and filtered prior to use. THF- d_8 was purchased from Sigma-Aldrich, dried over Sodium/Potassium alloy, and filtered prior to use.

Computational Methods

Density Functional theory (DFT) calculations were performed using the Gaussian 16 software package (revision C01).¹³ **2** was calculated as a cationic doublet with a 28 in-core electron pseudopotential (ECP28MDF) on both Y atoms.¹⁴ The best method for the characterization of **2** was determined by testing six unrestricted functionals: uB3LYP,¹⁵ uCAMB3LYP,¹⁶ uM06,¹⁷ uPBE0,¹⁸ uTPSS,¹⁹ and uTPSSh²⁰ using the def2-SVP basis set²¹ (retrieved through Basis Set Exchange^{22–24}) on all atoms. In all cases Grimmes D3 dispersion correction was implemented to account for dispersion effects.^{25,26} The computed bond metrics of all optimised structures were compared to those obtained experimentally (Table S2). The unrestricted TPSSh functional best represented the experimental structure based on mean square error (MSE), root-mean-square error (RMSE), and mean absolute percentage error (MAPE). Thus, a final geometry optimisation was completed employing the def2-TZVP description on the Y and N atoms. The minimum structure was confirmed through analytical frequency calculations (Figure S17 and Figure S19). To appropriately compare the computational data between **1** and **2**, the structure of **1** was optimised using the same description. All NBO and NLMO calculations were performed using the NBO 6 program.^{27,28} TDDFT calculations were carried out on the optimised structures of **1** and **2** for 50 excited states on the def2-SVP(C,H)/def2-TZVP(Y,N)/ECP28MDF(Y) level of theory using the unrestricted TPSSh functional with GD3 dispersion correction. A CPCM implicit solvent model for dichloromethane was included.^{29,30}

The optimised coordinates of **2** were subsequently used to calculate both the g - and A -tensors using the %EPRNMR block implemented in the ORCA 5.0.4 software^{31,32} using the uTPSSh functional employing Grimme's D3 dispersion correction reformulated with Becke-Johnson damping (D3BJ).^{33,34} The ZORA-def2-SVP basis set²¹ was used for all carbon and hydrogen atoms, ZORA-def2-TZVP basis set was used for the treatment of nitrogen atoms,²¹ and the SARC-def2-TZVP³⁵ description was used for the yttrium atoms. The calculations employed the SARC/J auxiliary basis.^{36,37} A dichloromethane Conductor-like Polarizable Continuum Model (CPCM) was also considered to account for solvation effects.³⁸ To speed up the construction of the Hartree-Fock matrices as well as the gradient/Hessian integrals, RIJCOSX method was applied.³⁹

Electrochemistry

All cyclic voltammetry experiments were conducted under an inert atmosphere in an argon-filled glovebox. Data were collected using a Metrohm Autolab PGSTAT204 potentiostat with a glassy carbon working electrode, platinum wire counter electrode, and platinum wire pseudoreference electrode. **1** was dissolved in a 250 mM solution of [NⁿBu₄][PF₆] in dichloromethane. The voltammograms were referenced externally to the ferrocene redox couple.

EPR Spectroscopy

All EPR spectra were recorded on a Bruker EMX-plus spectrometer operating at X-band frequencies. The spectrometer is equipped with a Bruker ER4119HS probe and a modified Bruker liquid nitrogen variable temperature accessory. The data for **2** were collected under the following conditions: microwave frequency, 9.32 GHz, microwave power, 5.02 mW; field modulation amplitude, 0.005 mT. Samples were prepared in quartz EPR tubes using a 2 mM solution of **2** in thoroughly dried dichloromethane. All simulations were performed employing the EasySpin 5.2.35 software package⁴⁰ for MATLAB.

X-Ray Crystallography

Table S1. Crystal data and structural refinement of $[(\text{Cp}^{\text{tet}}_2\text{Y})_2(\mu\text{-abpy})]$, **1**, and $[(\text{Cp}^{\text{tet}}_2\text{Y})_2(\mu\text{-abpy})](\text{BPh}_4)$, **2**. **2** crystallised with one dichloromethane and one and a half toluene molecules in the lattice as $[(\text{Cp}^{\text{tet}}_2\text{Y})_2(\mu\text{-abpy})](\text{BPh}_4)\cdot\text{CH}_2\text{Cl}_2\cdot 1.5\text{C}_7\text{H}_8$.

| Compound | 1 | 2 ·CH ₂ Cl ₂ ·1.5C ₇ H ₈ |
|---|---|--|
| Empirical formula | C ₄₆ H ₆₀ N ₄ Y ₂ | C _{81.5} H ₉₄ BCl ₂ N ₄ Y ₂ |
| CCDC Number | 2366736 | 2366737 |
| Formula weight (g mol ⁻¹) | 846.80 | 1389.13 |
| Temperature (K) | 100.0(1) | 100.2(1) |
| Crystal system | Monoclinic | Monoclinic |
| Space group | P2 ₁ /n | P2 ₁ /n |
| Unit Cell Dimensions | | |
| a (Å) | 9.44889(8) | 13.24606(13) |
| b (Å) | 17.36119(16) | 25.0683(2) |
| c (Å) | 12.52981(12) | 21.28315(17) |
| α (°) | 90 | 90 |
| β (°) | 97.9313(8) | 91.9119(8) |
| γ (°) | 90 | 90 |
| Volume (Å ³) | 2035.78(3) | 7063.26(11) |
| Z | 2 | 4 |
| ρ _{calc} (g cm ⁻³) | 1.381 | 1.306 |
| μ (mm ⁻¹) | 4.074 | 3.239 |
| F(000) | 884.0 | 2912 |
| Crystal size (mm ³) | 0.187 × 0.138 × 0.105 | 0.221 × 0.143 × 0.063 |
| Radiation | Cu Kα (λ = 1.54184) | Cu Kα (λ = 1.54184) |
| 2θ range for data collection (°) | 8.758 to 154.614 | 5.448 to 160.206 |
| Reflections collected | 26108 | 60595 |
| Independent reflections | 4239 R _{int} = 0.0629 | 15090 R _{int} = 0.0430 |
| Data/restraints/parameters | 4239/0/243 | 15090/746/1068 |
| Goodness-of-fit on F ² | 1.062 | 1.035 |
| Final R indexes [<i>I</i> > 2σ (<i>I</i>)] | R ₁ = 0.0422, wR ₂ = 0.1101 | R ₁ = 0.0546, wR ₂ = 0.1473 |
| Final R indexes [all data] | R ₁ = 0.0432, wR ₂ = 0.1109 | R ₁ = 0.0631, wR ₂ = 0.1539 |
| Largest diff. peak/hole (e Å ⁻³) | 1.25 /-1.09 | 0.64 /-1.40 |

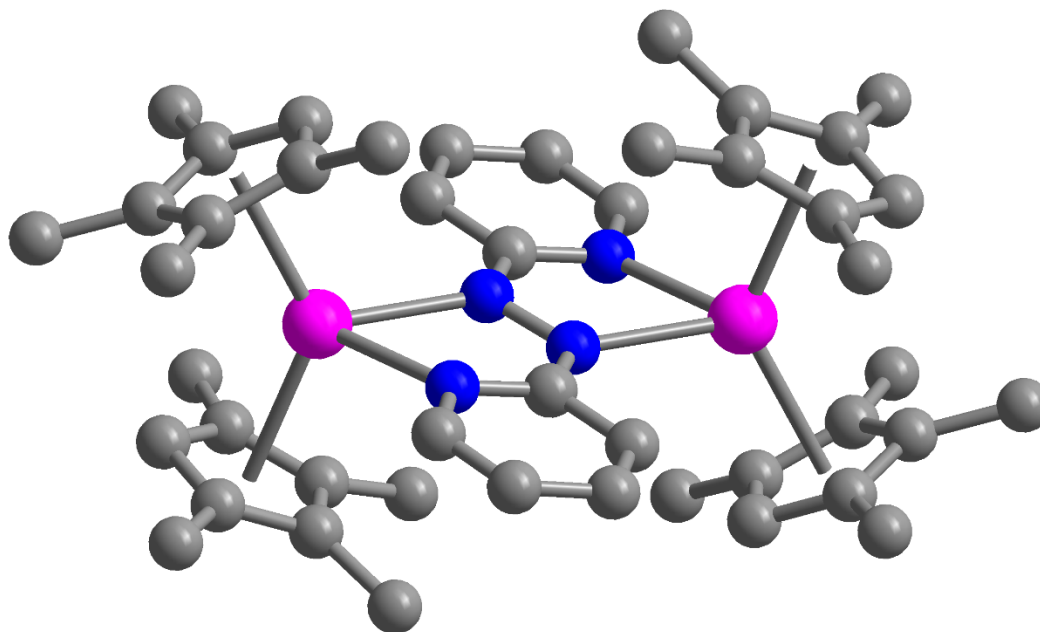


Figure S1. Structure of $[(\text{Cp}^{\text{tet}}_2\text{Y})_2(\mu\text{-abpy})]$, **1**. Pink, blue, and grey spheres represent Y, N, and C atoms, respectively. Hydrogen atoms have been omitted for clarity.

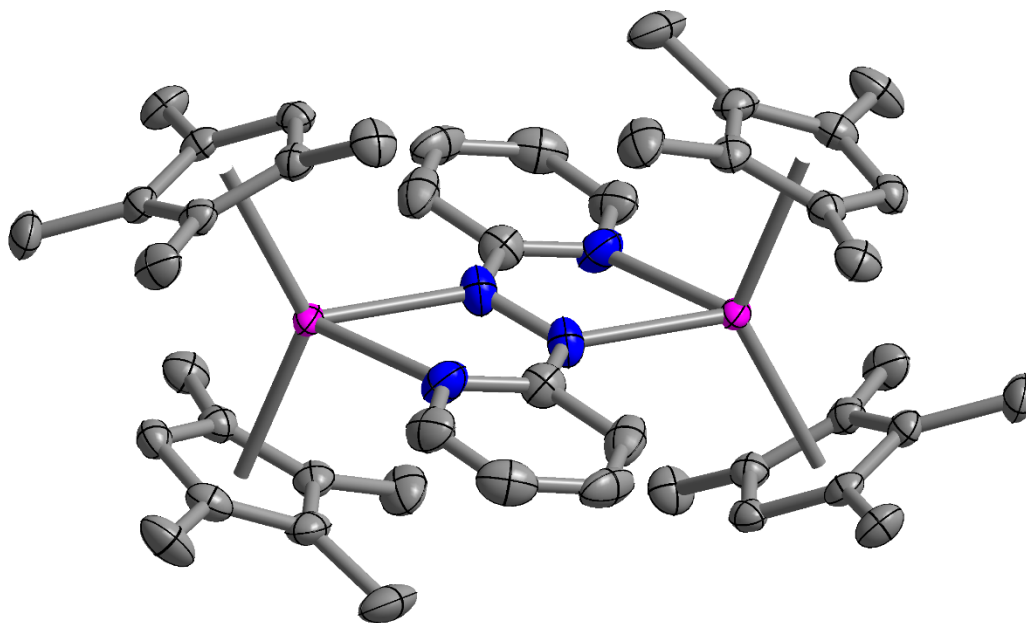


Figure S2. Structure of $[(\text{Cp}^{\text{tet}}_2\text{Y})_2(\mu\text{-abpy})]$, **1**, with thermal ellipsoids drawn at 50%. Pink, blue, and grey ellipsoids represent Y, N, and C atoms, respectively. Hydrogen atoms have been omitted for clarity.

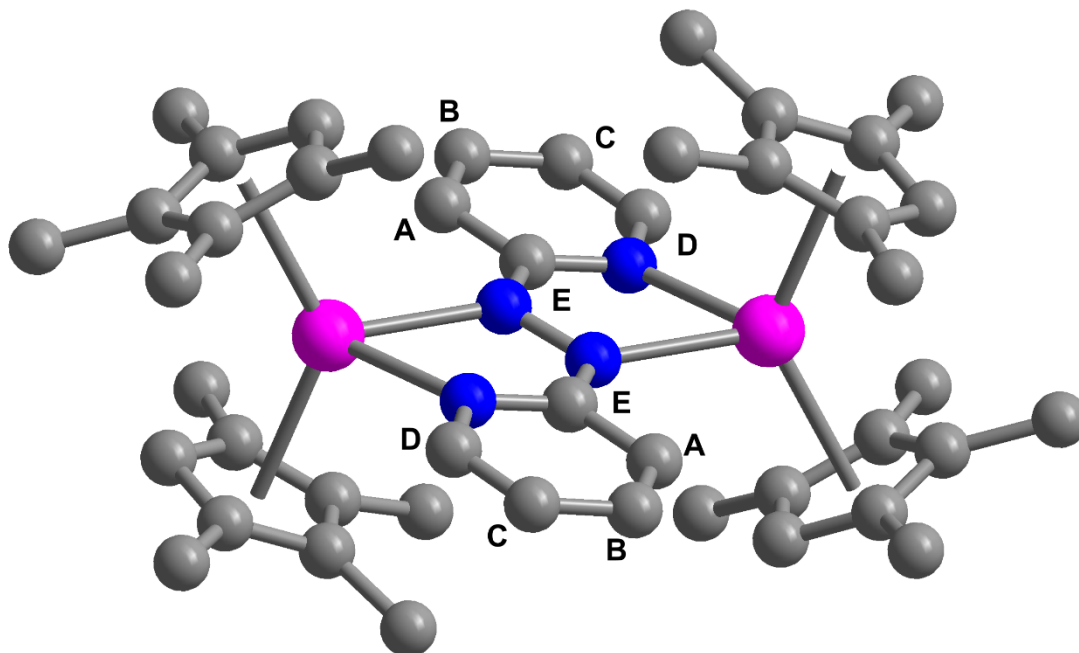


Figure S3. Structure of $[(\text{Cp}^{\text{tet}}_2\text{Y})_2(\mu\text{-abpy})]$, **1**, with relevant atom labels. Pink, blue, and grey spheres represent Y, N, and C atoms, respectively. Hydrogen atoms have been omitted for clarity.

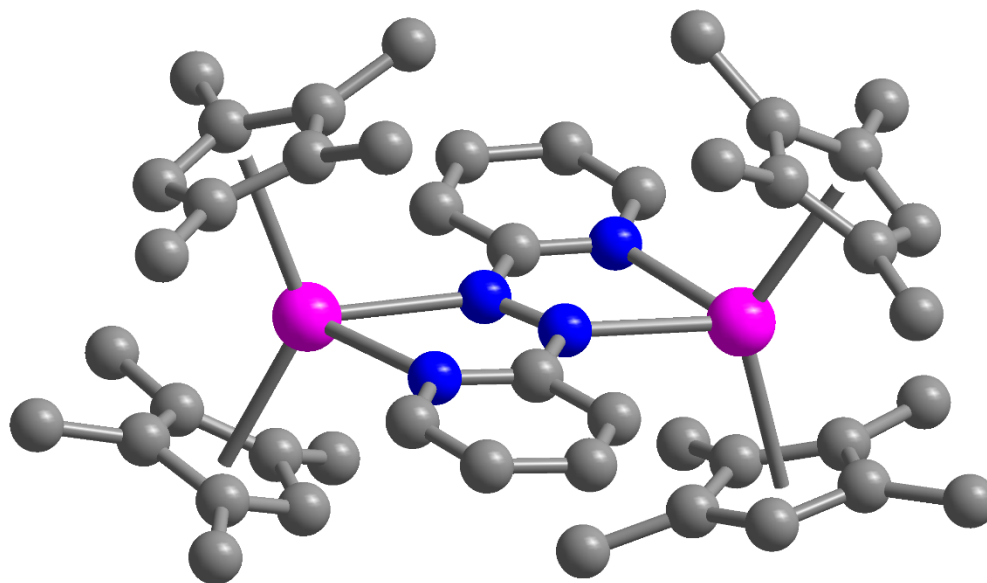


Figure S4. Structure of the cation of $[(\text{Cp}^{\text{tet}}_2\text{Y})_2(\mu\text{-abpy}^+)](\text{BPh}_4)$, **2**, in a crystal of $[(\text{Cp}^{\text{tet}}_2\text{Y})_2(\mu\text{-abpy}^+)](\text{BPh}_4) \cdot \text{CH}_2\text{Cl}_2 \cdot 1.5\text{C}_7\text{H}_8$. Pink, blue, and grey spheres represent Y, N, and C atoms, respectively. The $[\text{BPh}_4]^-$ counter ion, hydrogen atoms, and co-crystallised toluene and dichloromethane solvent molecules have been omitted for clarity.

NMR Spectroscopy

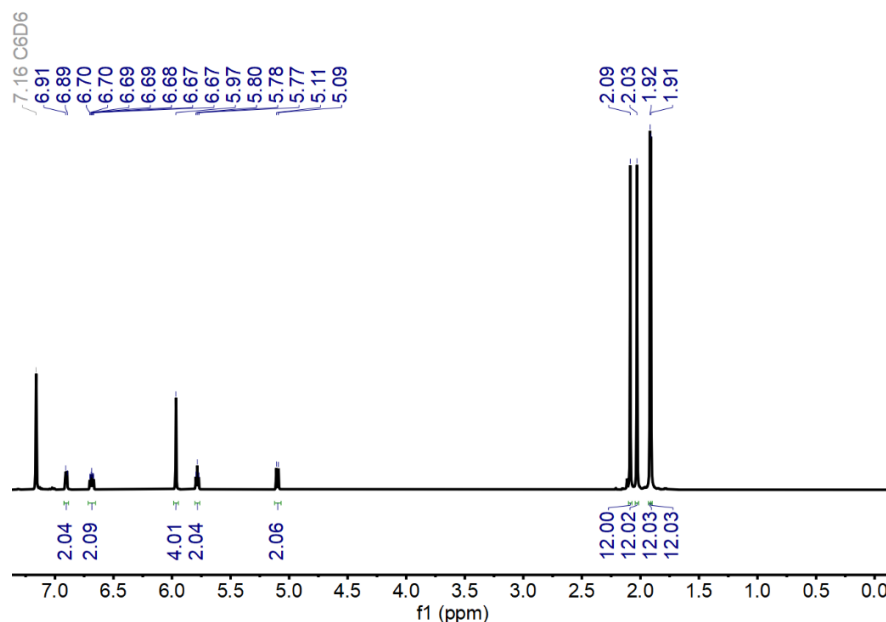


Figure S5. ^1H NMR spectrum of $[(\text{Cp}^{\text{tet}}_2\text{Y})_2(\mu\text{-abpy})]$, **1**, (500 MHz, ppm, benzene- d_6 , 25 °C): δ 1.91 (s, 12 H, $\text{C}_5\text{Me}_4\text{H}$), 1.92 (s, 12 H, $\text{C}_5\text{Me}_4\text{H}$), 2.03 (s, 12 H, $\text{C}_5\text{Me}_4\text{H}$), 2.09 (s, 12 H, $\text{C}_5\text{Me}_4\text{H}$), 5.10 (d, $^3J_{\text{H-H}} = 8.85$ Hz, 2 H, abpy- H_A), 5.78 (t, $^3J_{\text{H-H}} = 6.24$ Hz, 2 H, abpy- H_C), 5.97 (s, 4 H, $\text{C}_5\text{Me}_4\text{H}$), 6.69 (td, $^3J_{\text{H-H}} = 7.54$ Hz, $^4J_{\text{H-H}} = 1.61$ Hz, 2 H, abpy- H_B), 6.90 (d, $^3J_{\text{H-H}} = 5.78$ Hz, 2 H, abpy- H_D). See Figure S3 for relevant atom labels.

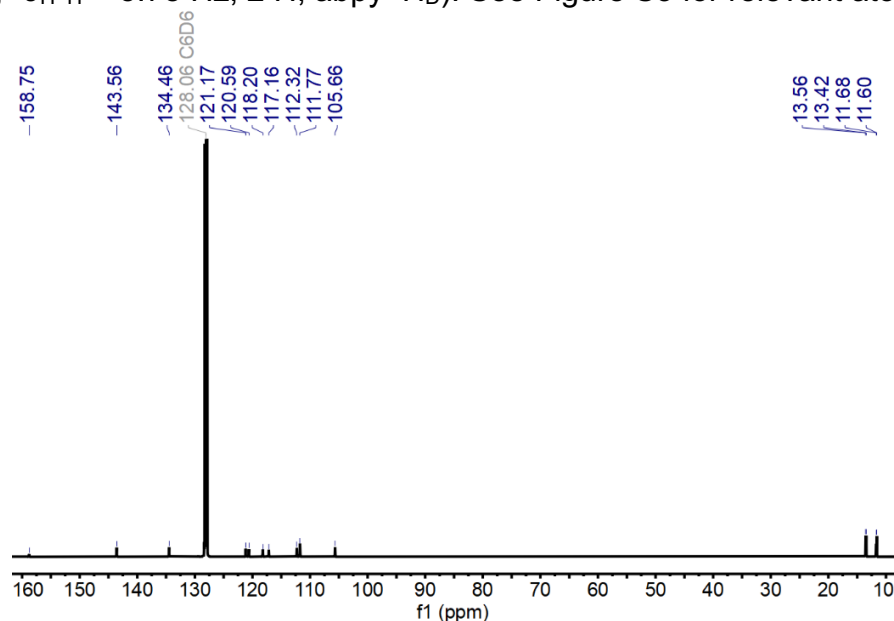


Figure S6. ^{13}C NMR spectrum of $[(\text{Cp}^{\text{tet}}_2\text{Y})_2(\mu\text{-abpy})]$, **1**, (126 MHz, ppm, benzene- d_6 , 25 °C): δ 11.60 ($\text{C}_5\text{Me}_4\text{H}$), 11.68 ($\text{C}_5\text{Me}_4\text{H}$), 13.42 ($\text{C}_5\text{Me}_4\text{H}$), 13.65 ($\text{C}_5\text{Me}_4\text{H}$), 105.66 (abpy- C_C), 111.77 (abpy- C_E), 112.32 (abpy- C_A), 117.16 ($\text{C}_5\text{Me}_4\text{H}$), 118.20 ($\text{C}_5\text{Me}_4\text{H}$), 120.59 ($\text{C}_5\text{Me}_4\text{H}$), 121.17 ($\text{C}_5\text{Me}_4\text{H}$), 134.46 (abpy- C_B), 143.56 (abpy- C_D), 158.75 ($\text{C}_5\text{Me}_4\text{H}$). See Figure S3 for relevant atom labels.

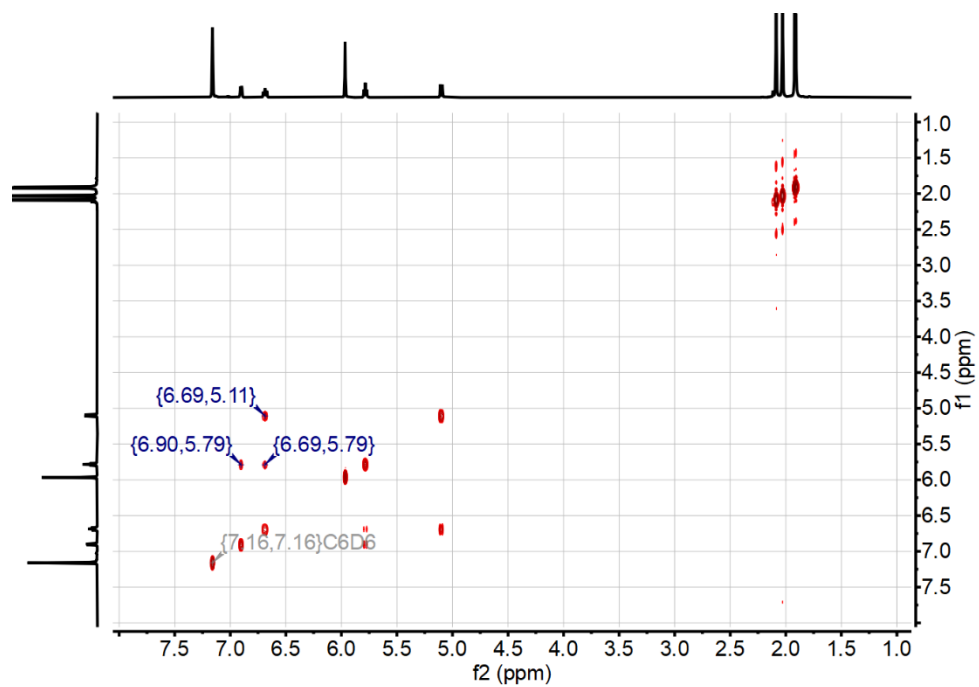


Figure S7. ^1H - ^1H gCOSY spectrum of $[(\text{Cp}^{\text{tet}}_2\text{Y})_2(\mu\text{-abpy})]$, **1**, (500 MHz, benzene- d_6 , 25 $^\circ\text{C}$).

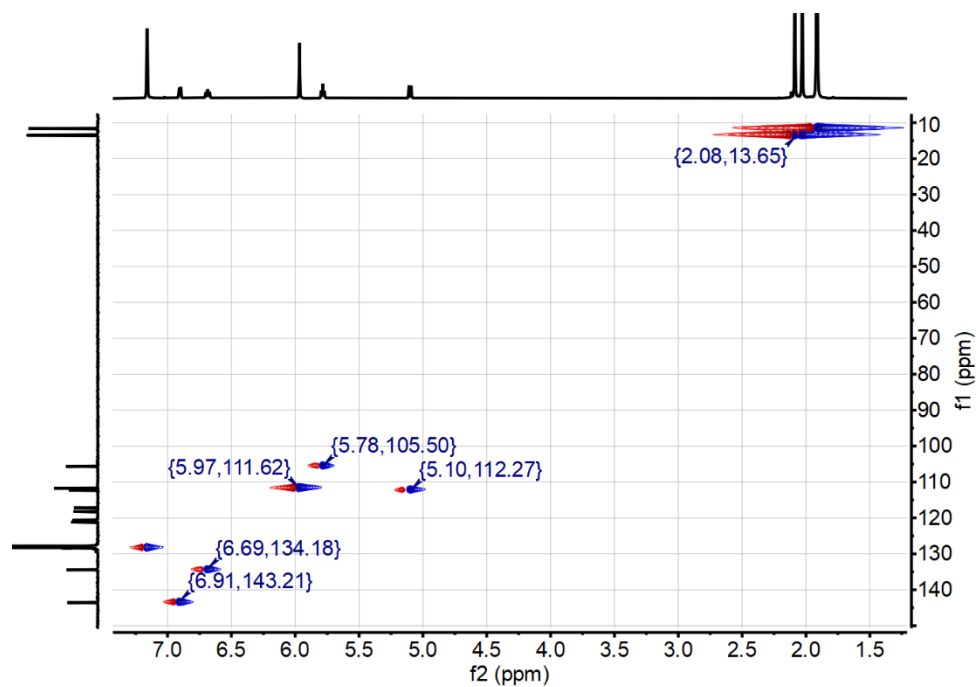


Figure S8. ^1H - ^{13}C gHSQC spectrum of $[(\text{Cp}^{\text{tet}}_2\text{Y})_2(\mu\text{-abpy})]$, **1**, (500 MHz, benzene- d_6 , 25 $^\circ\text{C}$).

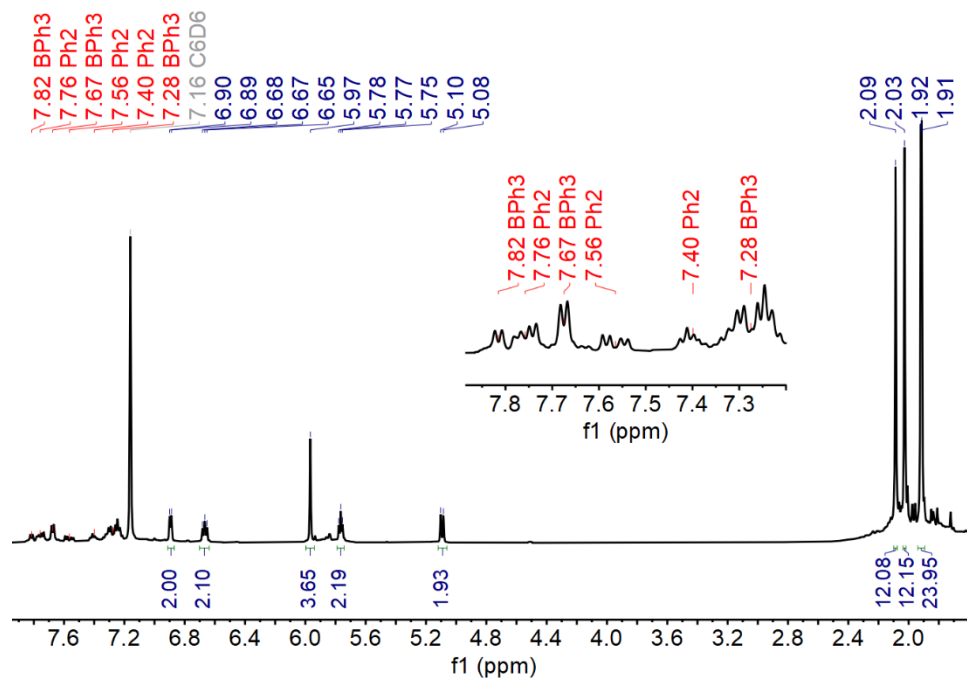


Figure S9. ^1H NMR spectrum of the crude reaction mixture for the synthesis of $[(\text{Cp}^{\text{tet}}_2\text{Y})_2(\mu\text{-abpy})]$, **1**, (500 MHz, ppm, benzene- d_6 , 25 °C). The peaks in the aromatic region are attributed to the reduction products of the $[\text{BPh}_4]^-$ anion, biphenyl and BPh_3 .

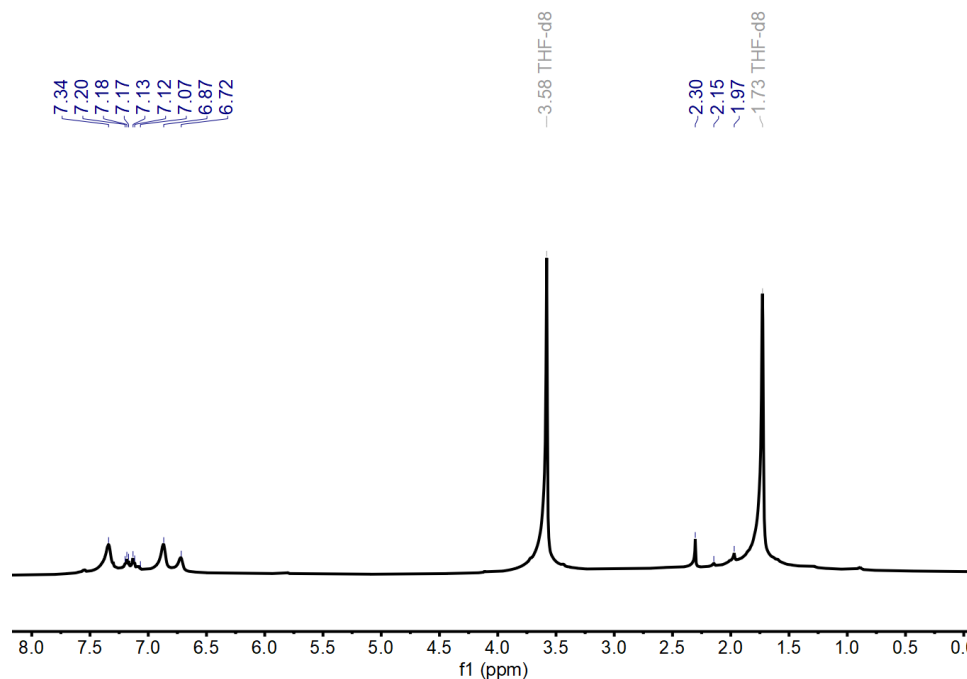


Figure S10. ^1H NMR spectrum of $[(\text{Cp}^{\text{tet}}_2\text{Y})_2(\mu\text{-abpy}')](\text{BPh}_4)$, **2**, (500 MHz, ppm, THF- d_8 , 25 °C): δ 7.34, 7.20, 7.18, 7.17, 7.13, 7.12, 7.07, 6.87, 6.72, 2.30, 2.15, 1.97, 1.73.

IR Spectroscopy

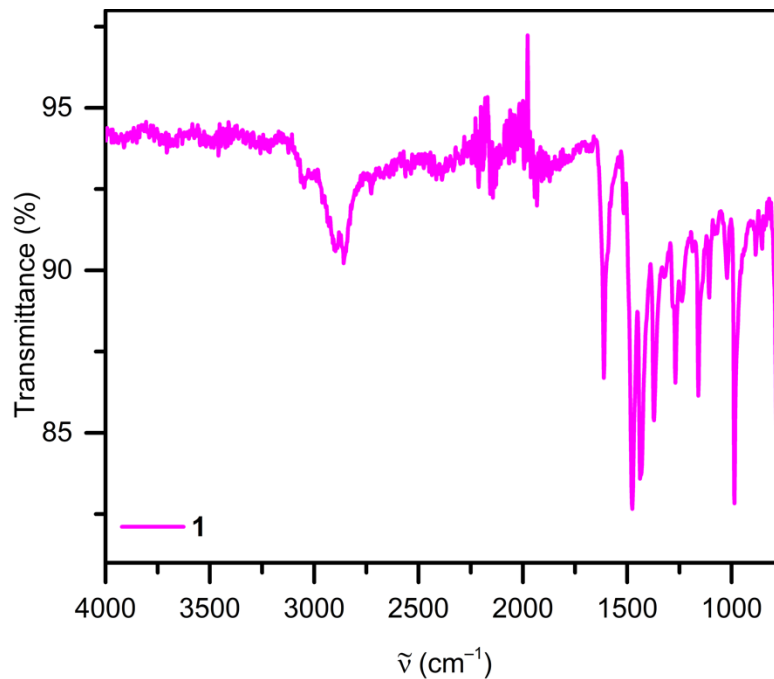


Figure S11. FTIR spectrum of $[(\text{Cp}^{\text{tet}}_2\text{Y})_2(\mu\text{-abpy})]$, **1**.

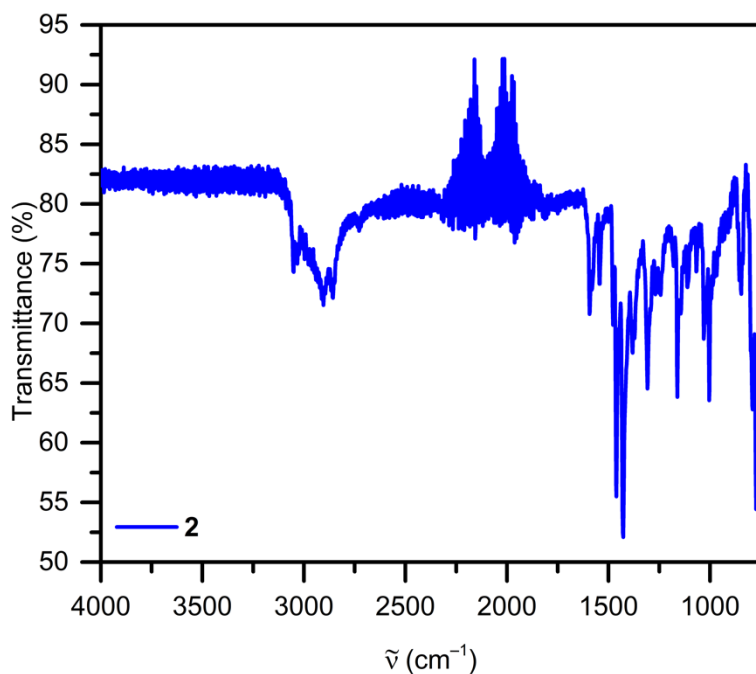


Figure S12. FTIR spectrum of $[(\text{Cp}^{\text{tet}}_2\text{Y})_2(\mu\text{-abpy}^*)](\text{BPh}_4)$, **2**.

UV-vis Spectroscopy

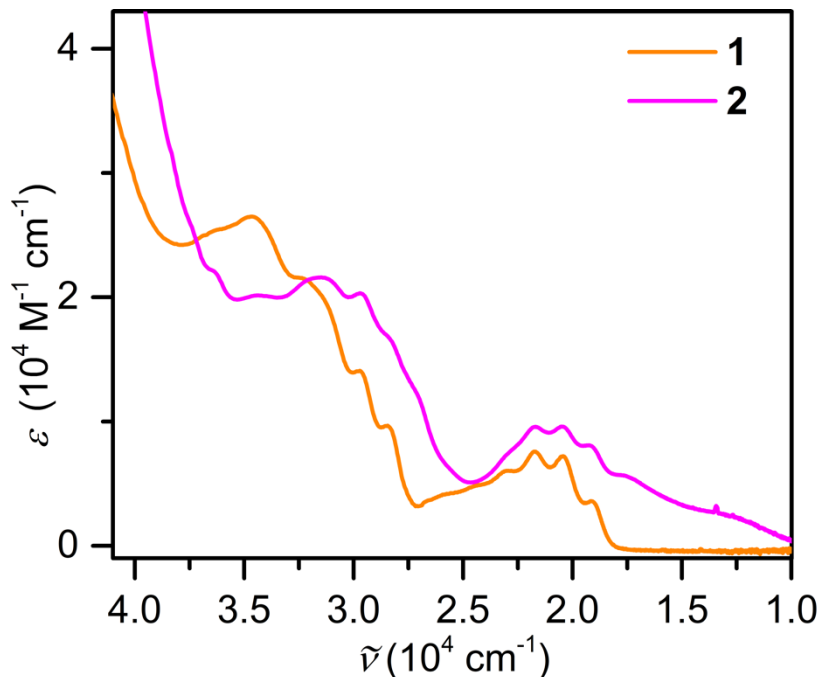


Figure S13. UV-vis absorption spectrum of $[(\text{Cp}^{\text{tet}_2\text{Y}})_2(\mu\text{-abpy})]$, **1** (orange), and $[(\text{Cp}^{\text{tet}_2\text{Y}})_2(\mu\text{-abpy}^*)](\text{BPh}_4)$, **2** (pink). Measurements were performed in dichloromethane solutions at $15 \mu\text{M}$.

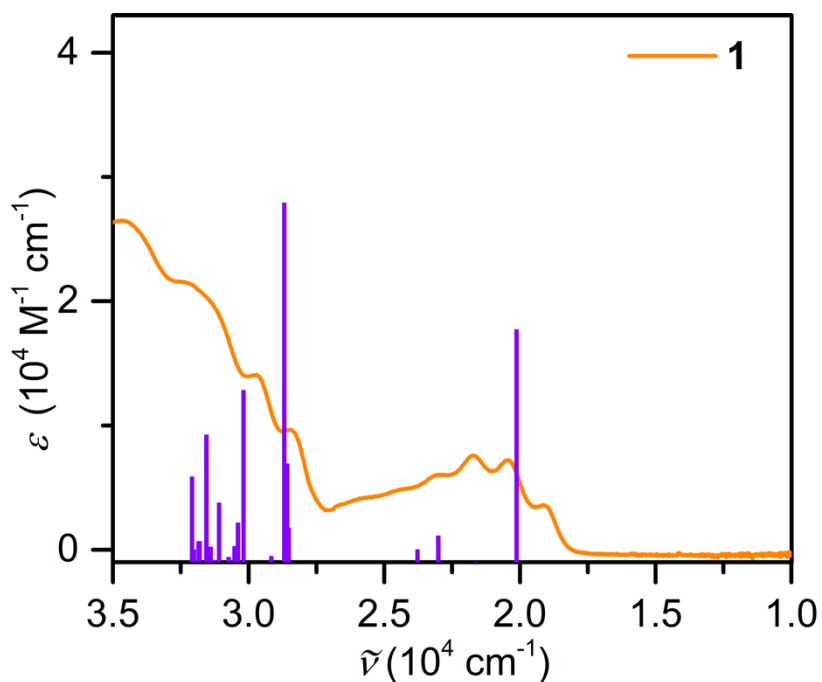


Figure S14. UV-vis absorption spectrum of $[(\text{Cp}^{\text{tet}_2\text{Y}})_2(\mu\text{-abpy})]$, **1**. The orange line represents experimental data for **1**, whereas the purple lines constitute calculated TDDFT transitions. Measurements were performed in dichloromethane solutions at $15 \mu\text{M}$.

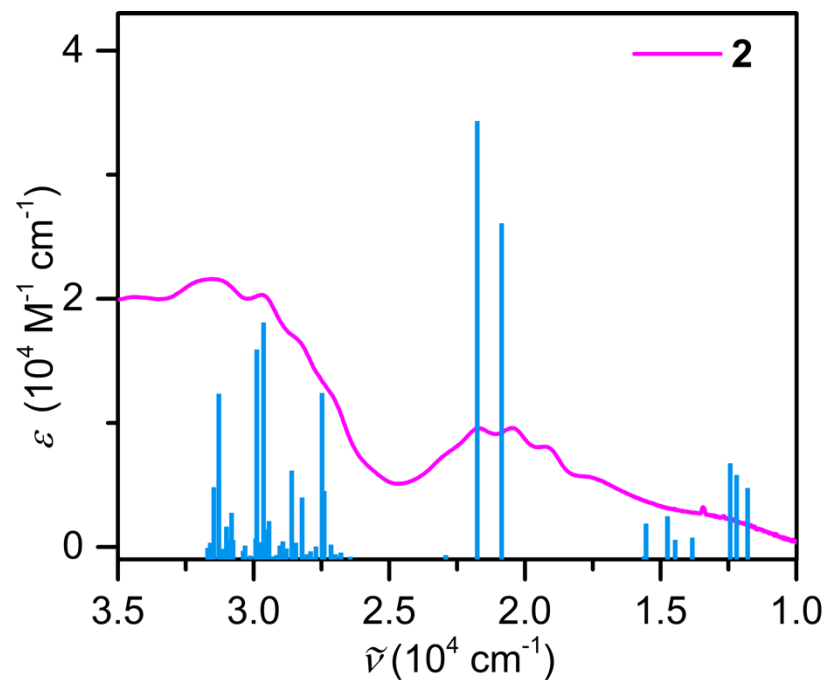


Figure S15. UV-vis absorption spectrum of $[(\text{Cp}^{\text{tet}}_2\text{Y})_2(\mu\text{-abpy}^*)](\text{BPh}_4)$, **2**. The pink line represents experimental data for **2**, whereas the light blue lines constitute calculated TDDFT transitions. Measurements were performed in dichloromethane solutions at 15 μM .

Cyclic Voltammetry

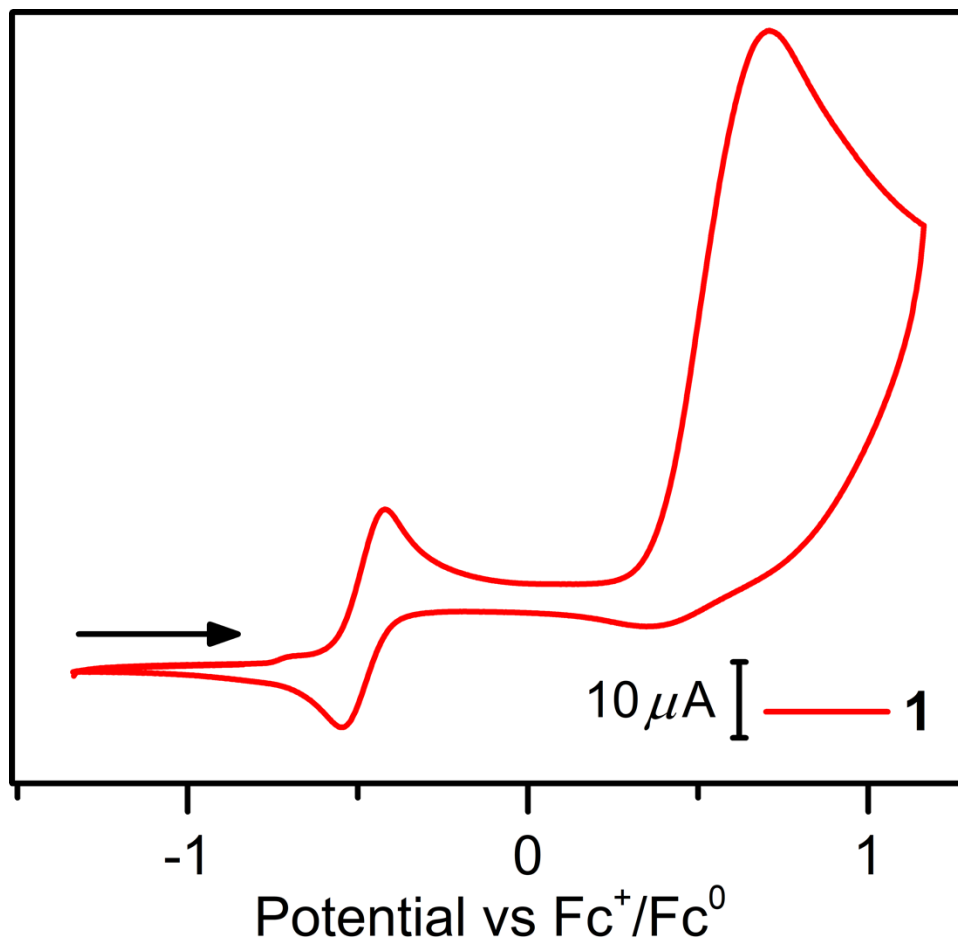


Figure S16. Cyclic voltammogram of $[(\text{Cp}^{\text{tet}}_2\text{Y})_2(\mu\text{-abpy})]$, **1**, vs. Fc. Measurements were taken in 250 mM $[\text{nBu}_4\text{N}][\text{PF}_6]$ in dichloromethane with analyte concentration of 3 mM. Measurements were conducted under 100 mV/s scan rates. One reversible (-489 mV) and one irreversible (660 mV) redox events are observed (Fc. redox couple at 836 mV).

DFT Calculations

Table S2. Computed and average experimental bond metrics of $[(\text{Cp}^{\text{tet}}\text{Y})_2(\mu\text{-abpy})](\text{BPh}_4)$, **2**, with six different functionals using the def2-SVP basis set and a 28 electron ECP on Y. Relevant atoms selected to better gauge the metal 2,2'-azobispyridine.

| | Experimental (Å) | Calculated | | | | | |
|------------------------------------|------------------|------------|--------|--------|--------|--------|---------------|
| | | uB3LYP | uCAM | uM06 | uPBE0 | uTPSS | uTPSSh |
| Distances (Å) | | | | | | | |
| Y _{Y1} -N _{N2} | 2.378 | 2.427 | 2.429 | 2.430 | 2.423 | 2.417 | 2.420 |
| Y _{Y1} -N _{N1} | 2.425 | 2.463 | 2.465 | 2.451 | 2.459 | 2.442 | 2.447 |
| Y _{Y2} -N _{N3} | 2.428 | 2.469 | 2.469 | 2.453 | 2.466 | 2.449 | 2.453 |
| Y _{Y2} -N _{N4} | 2.389 | 2.432 | 2.433 | 2.437 | 2.428 | 2.423 | 2.425 |
| N _{N4} -C _{C35} | 1.360 | 1.345 | 1.340 | 1.340 | 1.339 | 1.353 | 1.347 |
| C _{C2} -N _{N4} | 1.366 | 1.359 | 1.348 | 1.352 | 1.352 | 1.368 | 1.361 |
| C _{C2} -C _{C10} | 1.405 | 1.417 | 1.409 | 1.411 | 1.412 | 1.421 | 1.416 |
| C _{C10} -C _{C21} | 1.362 | 1.385 | 1.380 | 1.381 | 1.382 | 1.389 | 1.385 |
| C _{C21} -C _{C38} | 1.394 | 1.406 | 1.400 | 1.401 | 1.401 | 1.412 | 1.407 |
| C _{C35} -C _{C38} | 1.392 | 1.389 | 1.384 | 1.386 | 1.387 | 1.394 | 1.390 |
| N _{N1} -C _{C2} | 1.376 | 1.373 | 1.375 | 1.368 | 1.367 | 1.373 | 1.371 |
| N _{N1} -N _{N3} | 1.352 | 1.338 | 1.326 | 1.327 | 1.324 | 1.351 | 1.340 |
| N _{N3} -C _{C1} | 1.374 | 1.372 | 1.374 | 1.367 | 1.367 | 1.372 | 1.370 |
| C _{C1} -C _{C14} | 1.408 | 1.417 | 1.410 | 1.411 | 1.412 | 1.422 | 1.417 |
| C _{C14} -C _{C37} | 1.356 | 1.385 | 1.380 | 1.380 | 1.382 | 1.389 | 1.385 |
| C _{C24} -C _{C37} | 1.386 | 1.406 | 1.400 | 1.402 | 1.402 | 1.412 | 1.407 |
| C _{C13} -C _{C24} | 1.385 | 1.389 | 1.383 | 1.386 | 1.386 | 1.394 | 1.390 |
| N _{N2} -C _{C13} | 1.358 | 1.344 | 1.340 | 1.340 | 1.339 | 1.353 | 1.347 |
| N _{N2} -C _{C1} | 1.356 | 1.359 | 1.348 | 1.352 | 1.352 | 1.370 | 1.362 |
| | MD | 0.018 | 0.018 | 0.017 | 0.018 | 0.015 | 0.015 |
| | MAD | 0.0118 | 0.0075 | 0.0066 | 0.0068 | 0.0133 | 0.0100 |
| | MSE | 5.4E-4 | 5.7E-4 | 4.9E-4 | 5.0E-4 | 3.7E-4 | 3.6E-4 |
| | RMSE | 2.3E-2 | 2.4E-2 | 2.2E-2 | 2.2E-2 | 1.9E-2 | 1.9E-2 |
| | MAPE | 1.03% | 1.04% | 1.02% | 1.06% | 0.93% | 0.92% |

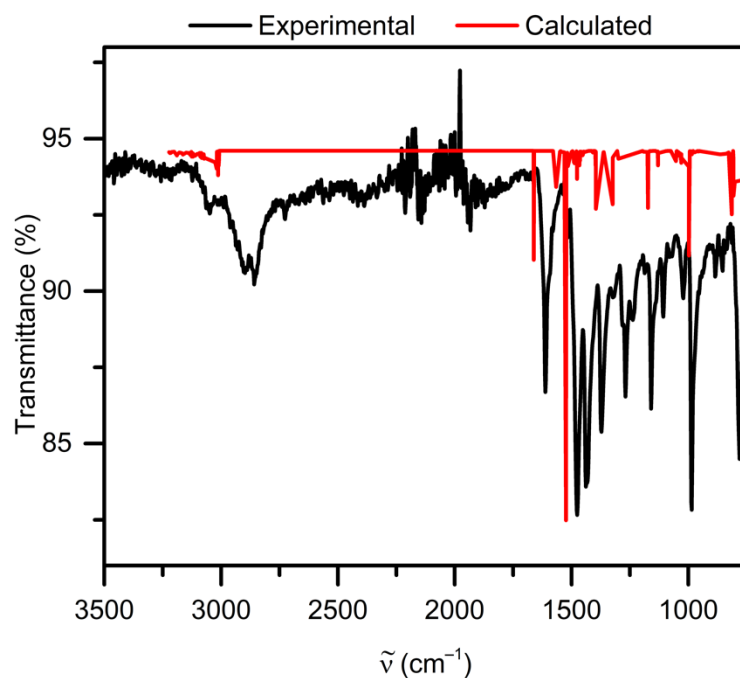


Figure S17. Comparison of experimental FTIR spectrum (black) and calculated stretching frequencies (red) of $[(\text{Cp}^{\text{tet}}_2\text{Y})_2(\mu\text{-abpy})]$, **1**.

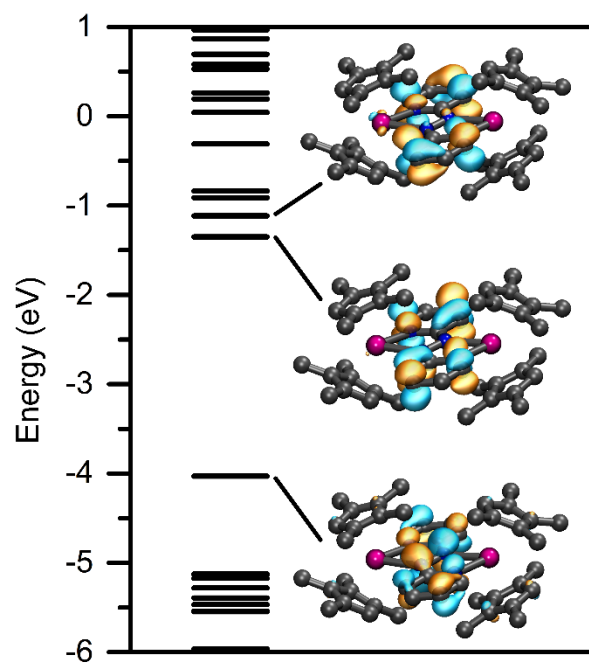


Figure S18. Calculated frontier orbitals of $[(\text{Cp}^{\text{tet}}_2\text{Y})_2(\mu\text{-abpy})]$, **1**, with the uTPSSH functional and def2-SVP(C,H)/def2-TZVP(Y,N) basis set. All isovalues were set to 0.4.

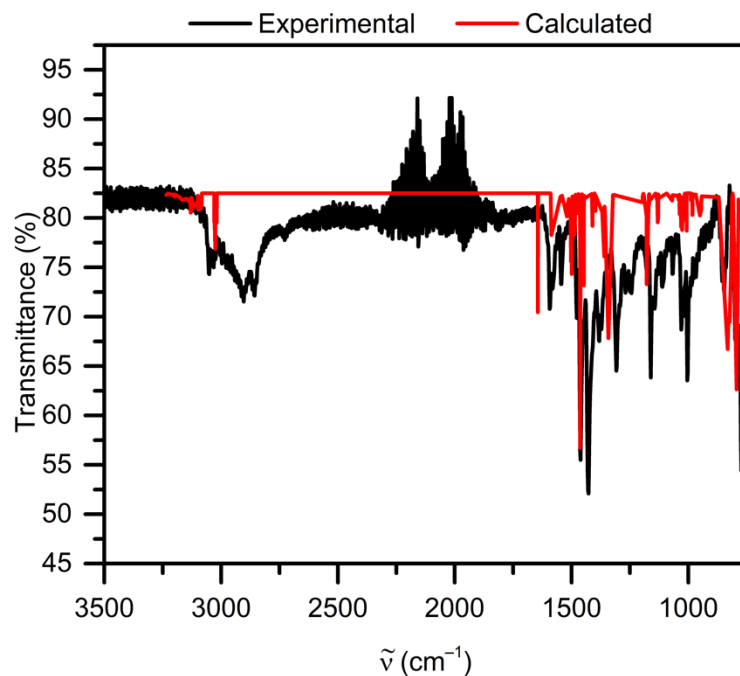


Figure S19. Comparison of experimental FTIR spectrum (black) and calculated stretching frequencies (red) of $[(\text{Cp}^{\text{tet}}_2\text{Y})_2(\mu\text{-abpy}^*)(\text{BPh}_4)]_2$, **2**.

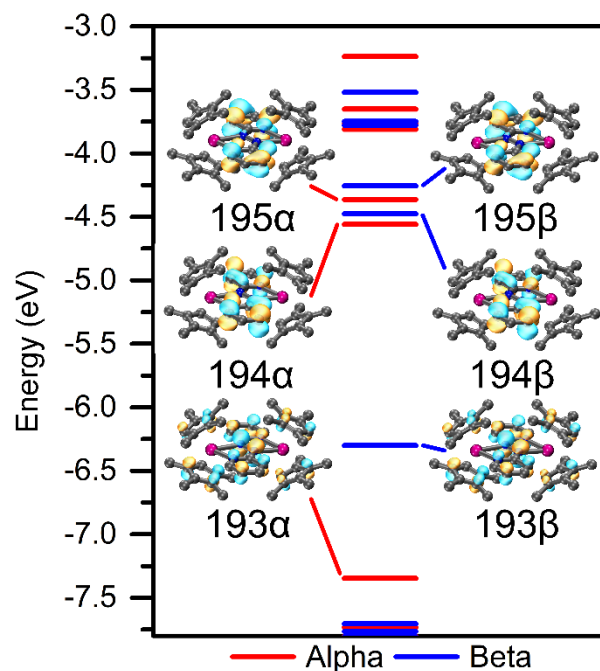


Figure S20. Calculated frontier orbitals of $[(\text{Cp}^{\text{tet}}_2\text{Y})_2(\mu\text{-abpy}^*)(\text{BPh}_4)]_2$, **2**, with the uTPSSh functional and def2-SVP(C,H)/def2-TZVP(Y,N) basis set. All isovalues were set to 0.4.

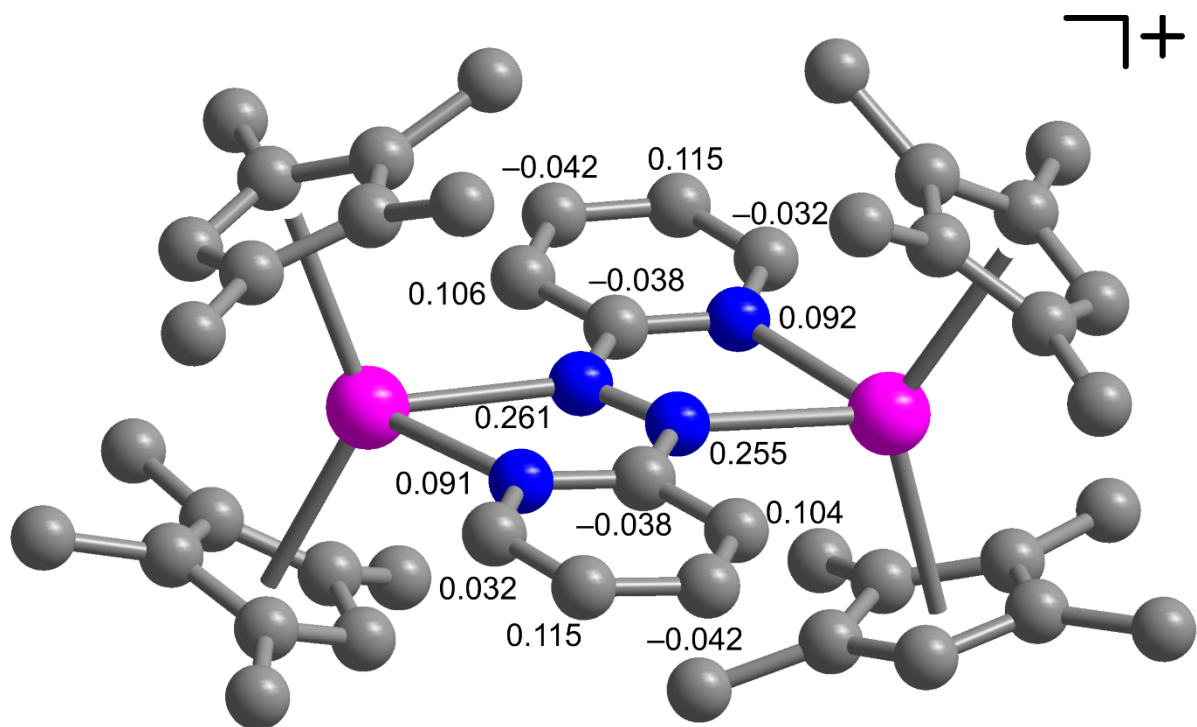
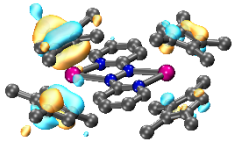
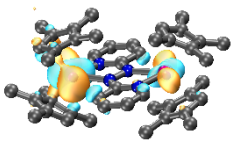
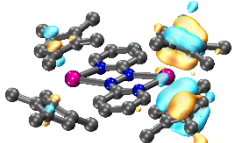
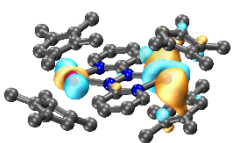
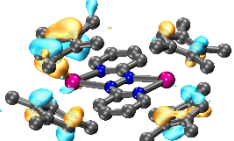
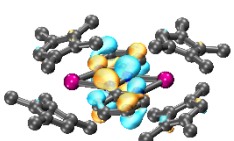
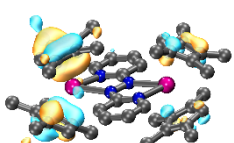
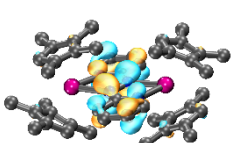
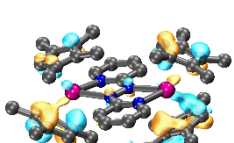
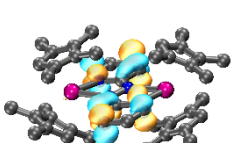
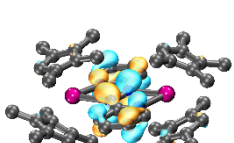
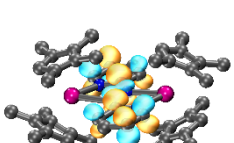


Figure S21. Calculated structure of $[(\text{Cp}^{\text{tet}}_2\text{Y})_2(\mu\text{-abpy})](\text{BPh}_4)$, **2**, with the uTPSSh functional and def2-SVP(C,H)/def2-TZVP(Y,N) basis set, with labeled Mulliken spin densities of the central abpy unit.

Table S3. Major contributions of the TDDFT-calculated transitions for $[(\text{Cp}^{\text{tet}}_2\text{Y})_2(\mu\text{-abpy})]$, **1**, on the def2-SVP(C,H)/def2-TZVP(Y,N)/ECP28MDF(Y) level using the uTPSSh functional with GD3 dispersion correction and dichloromethane implicit solvent model. Isovalue for all depictions is 0.04. Oscillator strength cutoff value: 0.02.

| λ (nm) | ν (cm^{-1}) | Oscillator Strength | Occupied | Virtual | Weight (%) |
|----------------|----------------------------|---------------------|--|--|------------|
| 312 | | 0.0696 |  192 |  197 | 45.9 |
| 317 | | 0.1038 |  191 |  196 | 57.4 |
| 321 | | 0.0484 |  190 |  195 | 68.9 |
| 329 | | 0.0321 |  192 |  195 | 67.8 |
| 331 | | 0.1402 |  189 |  194 | 66.6 |
| 349 | | 0.2930 |  193 |  198 | 55.0 |

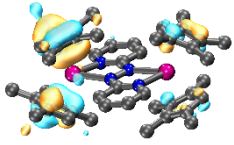
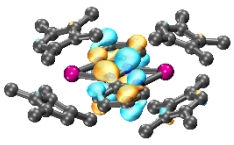
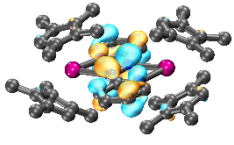
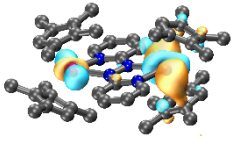
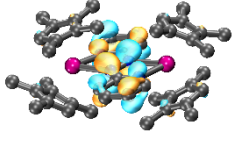
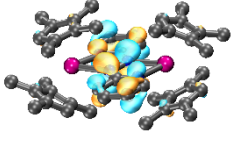
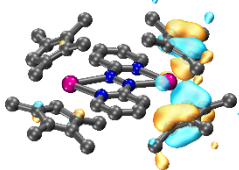
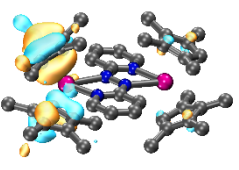
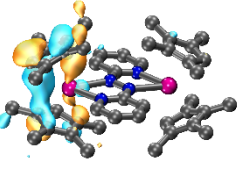
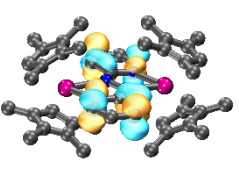
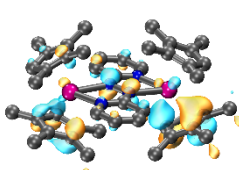
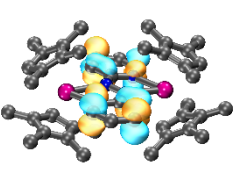
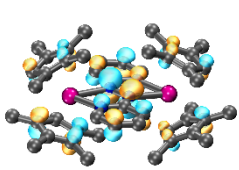
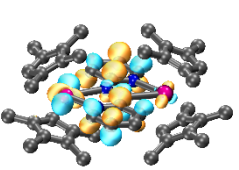
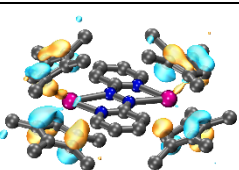
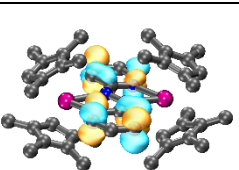
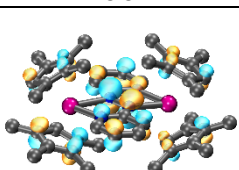
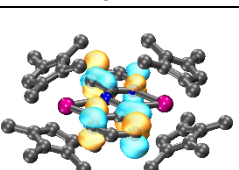
| | | | | | |
|-----|--|--------|--|--|------|
| 351 | | 0.0278 |  192 |  194 | 65.6 |
| 435 | | 0.0215 |  193 |  196 | 70.2 |
| 497 | | 0.1897 |  193 |  194 | 70.0 |

Table S4. Major contributions of the TDDFT-calculated transitions for $[(\text{Cp}^{\text{tet}}\text{Y})_2(\mu\text{-abpy})](\text{BPh}_4)$, **2**, on the def2-SVP(C,H)/def2-TZVP(Y,N)/ECP28MDF(Y) level using the uTPSSh functional with GD3 dispersion correction and dichloromethane implicit solvent model. The calculated excitation energies were empirically shifted by 0.2 eV. Isovalue for all depictions is 0.04. Oscillator strength cutoff value: 0.03.

| λ (nm) | ν (cm^{-1}) | Oscillator Strength | Occupied | Virtual | Weight (%) |
|----------------|----------------------------|---------------------|---|---|------------|
| 337 | | 0.0666 |  192A |  196A | 50.8 |
| 354 | | 0.0844 |  188B |  194B | 70.6 |
| 357 | | 0.0953 |  187A |  194A | 54.2 |
| 371 | | 0.0357 |  193A |  198A | 55.1 |
| 387 | | 0.0669 |  190A |  194A | 54.9 |
| 496 | | 0.1764 |  193A |  194A | 91.0 |

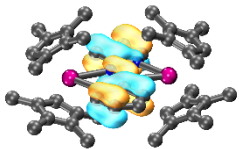
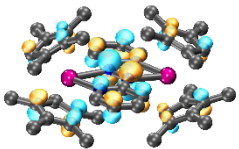
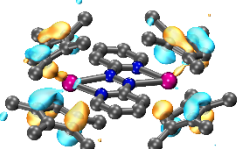
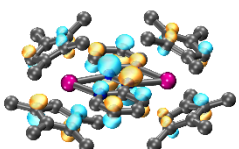
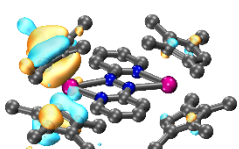
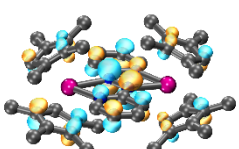
| | | | | | |
|-----|--|--------|---|---|------|
| 520 | | 0.1352 |  184B |  193B | 91.2 |
| 924 | | 0.0386 |  190B |  193B | 96.8 |
| 944 | | 0.0339 |  191B |  193B | 96.4 |

Table S5. Comparison of the DFT-calculated hyperfine coupling constants and the experimentally determined hyperfine coupling constants obtained from simulating the cw-EPR spectra of $[(\text{Cp}^{\text{tet}}\text{Y})_2(\mu\text{-abpy}^*)](\text{BPh}_4)$, **2**.

| | Calculated (MHz) | Experimental (MHz) |
|-----------------|------------------|--------------------|
| ^{89}Y | 3.92 and 4.23 | 4.08 |
| ^{14}N | 11.82 and 11.68 | 15.79 |
| ^{14}N | 3.81 and 3.88 | 4.82 |

References

- 1 W. J. Evans, D. S. Lee, M. A. Johnston and J. W. Ziller, *Organometallics*, 2005, **24**, 6393–6397.
- 2 B. J. Barker and P. G. Sears, *J. Phys. Chem.*, 1974, **78**, 2687–2688.
- 3 D. E. Bergbreiter and J. M. Killough, *J. Am. Chem. Soc.*, 1978, **100**, 2126–2134.
- 4 W. Fang, X. Liu, Z. Lu and T. Tu, *Chem. Commun.*, 2014, **50**, 3313–3316.
- 5 I. M. Piglosiewicz, R. Beckhaus, G. Wittstock, W. Saak and D. Haase, *Inorg. Chem.*, 2007, **46**, 7610–7620.
- 6 S. E. Lorenz, B. M. Schmiede, D. S. Lee, J. W. Ziller and W. J. Evans, *Inorg. Chem.*, 2010, **49**, 6655–6663.
- 7 M. R. MacDonald, J. W. Ziller and W. J. Evans, *Inorg. Chem.*, 2011, **50**, 4092–4106.
- 8 CrysAlisPro Software System Rigaku Corporation, Oxford 2020.
- 9 SCALE3 ABSPACK Empirical Absorption Correction, CrysAlis Pro - Software Package Rigaku Corporation, Oxford 2020.
- 10 G. Sheldrick, *Acta Crystallogr. Sect. A*, 2015, **71**, 3–8.
- 11 G. Sheldrick, *Acta Crystallogr. Sect. C*, 2015, **71**, 3–8.
- 12 O. V. Dolomanov, L. J. Bourhis, R. J. Gildea, J. A. K. Howard and H. Puschmann, *J. Appl. Crystallogr.*, 2009, **42**, 339–341.
- 13 Gaussian 16, Revision C.01, M. J. Frisch, G. W. Trucks, H. B. Schlegel, G. E. Scuseria, M. A. Robb, J. R. Cheeseman, G. Scalmani, V. Barone, G. A. Petersson, H. Nakatsuji, X. Li, M. Caricato, A. V. Marenich, J. Bloino, B. G. Janesko, R. Gomperts, B. Mennucci, H. P. Hratchian, J. V. Ortiz, A. F. Izmaylov, J. L. Sonnenberg, D. Williams-Young, F. Ding, F. Lipparini, F. Egidi, J. Goings, B. Peng, A. Petrone, T. Henderson, D. Ranasinghe, V. G. Zakrzewski, J. Gao, N. Rega, G. Zheng, W. Liang, M. Hada, M. Ehara, K. Toyota, R. Fukuda, J. Hasegawa, M. Ishida, T. Nakajima, Y. Honda, O. Kitao, H. Nakai, T. Vreven, K. Throssell, J. A. Montgomery Jr., J. E. Peralta, F. Ogliaro, M. J. Bearpark, J. J. Heyd, E. N. Brothers, K. N. Kudin, V. N. Staroverov, T. A. Keith, R. Kobayashi, J. Normand, K. Raghavachari, A. P. Rendell, J. C. Burant, S. S. Iyengar, J. Tomasi, M. Cossi, J. M. Millam, M. Klene, C. Adamo, R. Cammi, J. W. Ochterski, R. L. Martin, K. Morokuma, O. Farkas, J. B. Foresman and D. J. Fox, 2016.
- 14 K. A. Peterson, D. Figgen, M. Dolg and H. Stoll, *J. Chem. Phys.*, 2007, **126**, 124101.
- 15 A. D. Becke, *J. Chem. Phys.*, 1993, **98**, 5648–5652.
- 16 T. Yanai, D. P. Tew and N. C. Handy, *Chem. Phys. Lett.*, 2004, **393**, 51–57.
- 17 Y. Zhao and D. G. Truhlar, *Theor. Chem. Acc.*, 2008, **120**, 215–241.
- 18 C. Adamo and V. Barone, *J. Chem. Phys.*, 1999, **110**, 6158–6170.
- 19 J. Tao, J. P. Perdew, V. N. Staroverov and G. E. Scuseria, *Phys. Rev. Lett.*, 2003, **91**, 146401.
- 20 V. N. Staroverov, G. E. Scuseria, J. Tao and J. P. Perdew, *J. Chem. Phys.*, 2003, **119**, 12129–12137.
- 21 F. Weigend and R. Ahlrichs, *Phys. Chem. Chem. Phys.*, 2005, **7**, 3297–3305.
- 22 K. L. Schuchardt, B. T. Didier, T. Elsethagen, L. Sun, V. Gurumoorthi, J. Chase, J. Li and T. L. Windus, *J Chem Inf Model*, 2007, **47**, 1045–1052.
- 23 B. P. Pritchard, D. Altarawy, B. Didier, T. D. Gibson and T. L. Windus, *J. Chem. Inf. Model.*, 2019, **59**, 4814–4820.

- 24 D. Feller, *J Comput Chem*, 1996, **17**, 1571–1586.
- 25 S. Grimme, J. Antony, S. Ehrlich and H. Krieg, *J. Chem. Phys.*, 2010, **132**, 154104.
- 26 D. G. A. Smith, L. A. Burns, K. Patkowski and C. D. Sherrill, *J. Phys. Chem. Lett.*, 2016, **7**, 2197–2203.
- 27 A. E. Reed and F. Weinhold, *J. Chem. Phys.*, 1985, **83**, 1736–1740.
- 28 E. D. Glendening, C. R. Landis and F. Weinhold, *J. Comput. Chem.*, 2013, **34**, 1429–1437.
- 29 V. Barone and M. Cossi, *J. Phys. Chem. A*, 1998, **102**, 1995–2001.
- 30 M. Cossi, N. Rega, G. Scalmani and V. Barone, *J. Comput. Chem.*, 2003, **24**, 669–681.
- 31 F. Neese, *WIREs Comput. Mol. Sci.*, 2012, **2**, 73–78.
- 32 F. Neese, *WIREs Comput. Mol. Sci.*, 2022, **12**, e1606.
- 33 S. Grimme, J. Antony, S. Ehrlich and H. Krieg, *J. Chem. Phys.*, 2010, **132**, 154104.
- 34 S. Grimme, S. Ehrlich and L. Goerigk, *J. Comput. Chem.*, 2011, **32**, 1456–1465.
- 35 J. D. Rolfes, F. Neese and D. A. Pantazis, *J. Comput. Chem.*, 2020, **41**, 1842–1849.
- 36 F. Weigend, *Phys. Chem. Chem. Phys.*, 2006, **8**, 1057.
- 37 D. A. Pantazis and F. Neese, *J. Chem. Theory Comput.*, 2009, **5**, 2229–2238.
- 38 V. Barone and M. Cossi, *J. Phys. Chem. A*, 1998, **102**, 1995–2001.
- 39 S. Kossmann and F. Neese, *J. Chem. Theory Comput.*, 2010, **6**, 2325–2338.
- 40 S. Stoll and A. Schweiger, *J. Magn. Reson.*, 2006, **178**, 42–55.